JOURNAL OF MATERIALS SCIENCE 33 (1998) 977–984

Hertzian flaw analysis and models for the prediction of flexural fracture strength of Al_2O_3 and Al_2O_3/SiC_p nanocomposites

C. C. ANYA
University of Oxford, Department of Materials, Parks Road, Oxford OX1 3PH, UK

A study is presented comparing the statistics of observed crack-originating flaws on fracture surfaces of samples of Al_2O_3 and its composites (having 5 and 15 vol % SiC particle, SiC_p) with those determined by the Hertzian indentation analysis. Cracks originating from Vickers microindents are also examined using transmission electron microscopy (TEM). Critical flaws determined by the Hertzian analysis predict experimental fracture strengths reasonably well when Orowan's model of obtaining the latter is used. This model is supported by microstructural features, which strongly suggest blunt crack-tips. The critical flaw sizes of alumina and the 5 vol % SiC_p composite are found to be practically the same. Hence the explanation of the higher strength of the composites (relative to alumina) based on flaw size is improbable. The composite with 15 vol % SiC_p is tougher and has a lower fracture strength in comparison with those of the 5 vol % SiC_p composite. Therefore an increase in toughness does not satisfactorily explain the strengthening trend. The change in the mode of fracture and the interspacing distances (implicitly the heights) of the fracture steps are suggested as the main factors that control strengthening in these materials.

1. Introduction

Previous studies [1–4] have shown that minor additions of SiC particles (SiC_p) in Al_2O_3, both nanometre-sized, lead to composites with flexutral strengths higher than that of monolithic alumina. The highest strength is conferred [1, 4] by 5 vol % SiC addition, Table I.

Some authors [1, 3] attribute the differences in strength to the sizes of critical flaws present in or on the surfaces of the materials, following Griffith's equations

$$\sigma_f = \frac{K_{1c}}{Y(C)^{1/2}} \quad (1)$$

Where σ_f is the fracture stress and K_{Ic} is the fracture toughness of the material. Y is a constant, which for a plane stress condition is equal to $(\pi)^{1/2}$ [7, 8] and C is the critical flaw size.

The average critical flaw sizes predicted by Equation 1 were found [4] to be between 20 and 31 μm. This is about 5–12 times greater than the average grain sizes [5] of the samples. Considering that the samples sintered to $\geqslant$ 99.6% of their theoretical density (TD), and with no agglomerations observed [5], it is doubtful how such well processed samples could have flaws of sizes far greater than their average grain size. Therefore it is necessary to study the nature of crack-originating flaws on fracture surfaces, and compare their sizes with those predicted by Griffth's equation and its offshoot, Orowan's model.

Hertzian indentation analysis, based on the concept of "searched area" [9], has been used [10] to compute the sizes of surface flaws. Because these flaws come to the surface by progressively grinding and polishing the samples towards their cores, the final flaws on the surface (prior to any test) will represent those from both stages of processing (intrinsic flaws), and the last surface preparation. It is worthwhile investigating how such flaws compare with those observed on fracture surfaces.

In this study, therefore, the critical flaws determined by the Hertzian indentation analysis are compared with those actually found on the fracture surfaces. The actual flaws and those determined analytically are also used to investigate which of the two models, Griffith's and Orowan's, very closely predicts the flexural strength of the materials. Finally, the concept of "fracture steps" is presented as the main factor responsible for the variation of strength in these materials.

2. Materials and experimental methods

The samples, alumina and the 5 and 15 vol % SiC "nanocomposites" of the present study, were pressureless sintered [5] to $\geqslant$ 99.6% TD. Four-point bend tests were carried out (with the tensile faces of the samples finish-polished to 1/4 μm diamond) following the procedure outlined in [4]. Table I is a summary of the characteristics of the materials. Fracture surfaces were examined using a Philips 501 scanning electron microscope (SEM). Hertzian indentations (of at least 25 in number, using 5 mm diameter alumina balls)

TABLE I Characteristics of materials used in the present study

SiC (vol %)	Grain size [7] (μm)	Density (% theoretical) [7]	σ_f [4] (MPa)	K_{Ic} (MPa m$^{-1/2}$) [6]
0[a]	3.5 ± 1.3	99.9	431 ± 53	3.5 ± 0.3
5	4.0 ± 1.1	99.8	646 ± 41	5.1 ± 0.8
15	2.6 ± 0.3	99.6	549 ± 30	5.4 ± 0.6

[a] This sample is composed entirely of Al_2O_3.

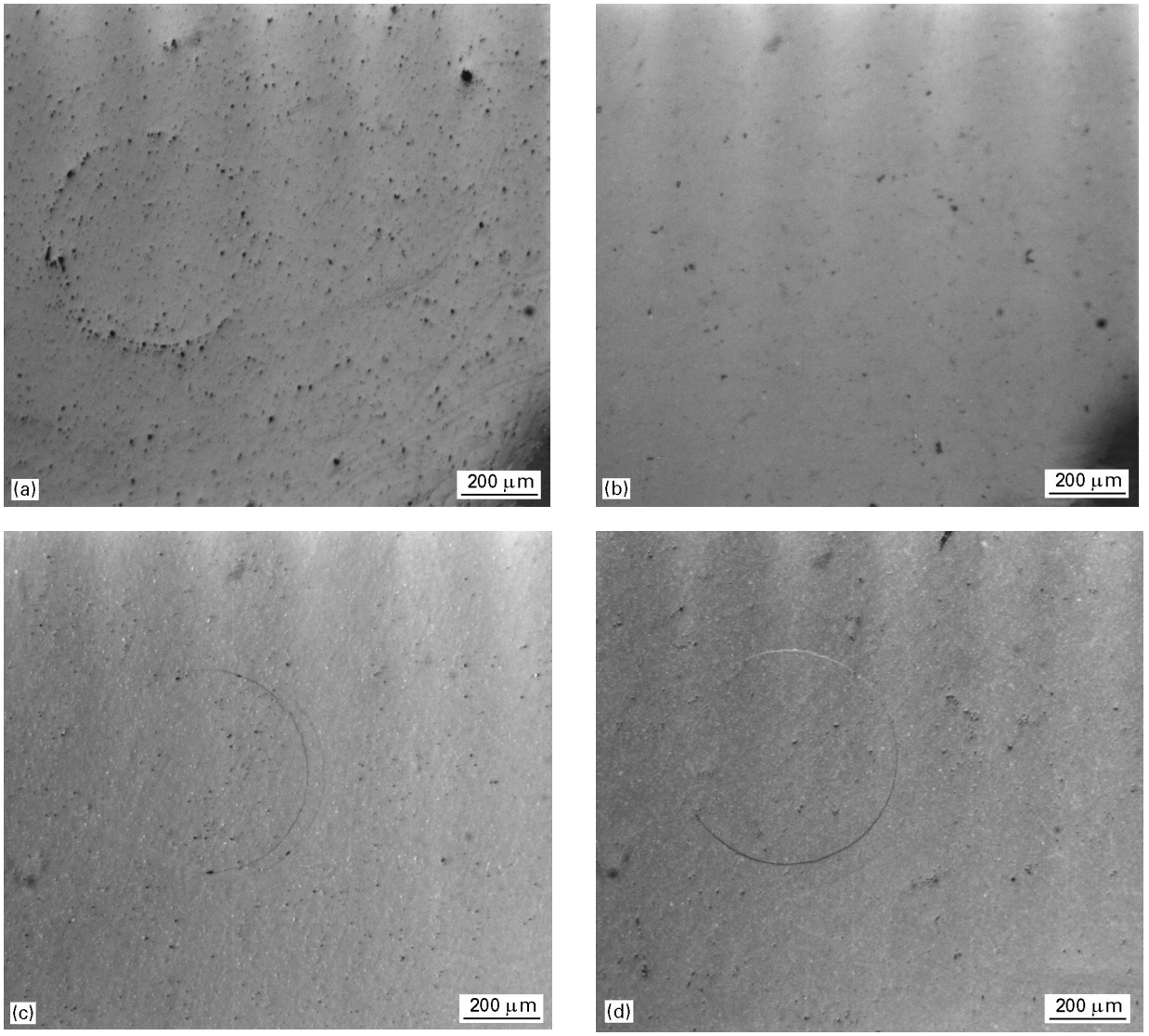

Figure 1 As-polished samples and typical ring cracks in: (a) Al_2O_3, etched and repolished (to 1 μm diamond) to reveal ring, (b) unetched 1/4 μm diamond polished Al_2O_3, (c) unetched 1/4 μm diamond polished 5 vol % SiC "nanocomposite", and (d) unetched 1/4 μm diamond polished 15 vol % SiC "nanocomposite".

were made on 1/4 μm diamond finish-polished samples. The same surface finish, therefore, makes it possible to relate the findings from the Hertzian method to those from four-point bent samples. A modified ET 500 testing machine (Engineering Systems, Nottingham) was used for the Hertzian indentation. Full details of the experimental procedure for the Hertzian indentation analysis can be found in [6].

The flaw sizes and densities from the Hertzian analysis were determined using computer simulations developed by Warren *et al.* [10] based on the principle of "searched area" [9].

To rationalize which of the two concepts, blunt and atomically sharp crack-tips, is more appropriate to adopt, cracks were introduced in the samples by Vickers microindentation. These were made with a 2 N load, on 200 μm thick, 3-mm diameter discs of the materials. The discs were polished from the reverse of the indented side down to about 50 μm. From the same reverse side the discs were dimpled to a thickness of about 20 μm, before being ion-milled (with Duomill Gatan) to produce a hole. Thinned samples were studied under the TEM (Philips CM20).

3. Results and discussions

3.1. Hertzian flaw analysis

Fig. 1 shows typical ring cracks for monolithic alumina (a, b), 5 vol % SiC (c) and 15 vol % SiC (d) composites. The rings in the materials are on unetched 1/4 μm diamond polished samples (see Fig. 1b for alumina in this state), but to reveal the ring in alumina the sample was etched and repolished to 1 μm diamond finish. Thus, it seems alumina (Fig. 1a) has far more flaws than the composites (Fig. 1c, d), but it does not. The sizes of the rings and the loads that produced them are used [6, 10] to compute the sizes, frequencies and densities of the flaws present in each of the materials (Fig. 2).

It can be seen that the frequencies of the largest (critical) flaw sizes are less than 10% for both alumina (5.16 μm) and for the 15 vol % SiC composite (6.52 μm), while the modal flaw sizes are between 2 and 5 μm for all the materials (Fig. 2a). The densities of the largest flaws are also relatively very low (Fig. 2b). The very high density of flaws up to 2 μm in size in the 15 vol % SiC composite is also worthy of note. This is due to the thermal expansion coefficient mismatch between alumina and SiC, which at a high volume fraction of particles, the matrix being under high tensile stress, leads [11] to submicrometre-sized flaws, as was frequently observed in the 15 vol % SiC composite in the present work. A typical example of such submicrometre-sized flaws observed in unbroken composites is shown in Fig. 3. They were rarely observed in the 5 vol % SiC composite.

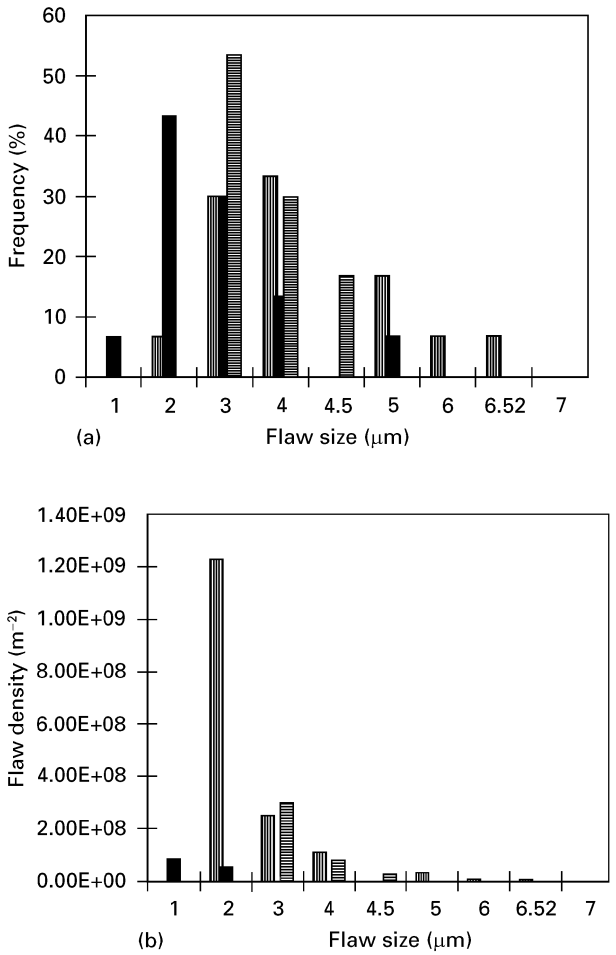

Figure 2 Histograms of flaws from the Hertzian indentation analysis for (a) frequency and (b) density versus flaw size: (▥) 15 vol % SiC, (■) alumina, (▤) 5 vol % SiC.

3.2. Flaws on fracture surfaces

The fracture surfaces of the materials are shown in Fig. 4. A wide area view is shown in Fig. 4a. Some of the flaws from which the cracks originate are indicated in Fig. 4a. The sizes of the flaws suggest that most of them are secondary. However, after a thorough examination of the surfaces, those shown in Fig. 4b are typical of the largest sizes observed. These measure about 3.8 ± 0.5 μm for alumina, and 3.5 ± 0.5 and 5 ± 0.4 μm for the 5 and 15 vol % composites, respectively.

3.3. Comparison of flaw statistics from both methods

The similarities and differences between the observed flaw sizes and those computed from the Hertzian analysis are noteworthy.

The small differences in the sizes of the largest flaws across the materials using both methods should be expected. Because the samples were surface finished to such a high degree (1/4 μm diamond), their largest flaws should result from the processing (sintering) of the material. Considering that all the materials are sintered to about the same degree of densification (Table I) all of them should have about the same size of largest flaws.

The material most disposed to flaws, and the most frequent sizes of flaws, in general, are also the same for both methods. It can be seen that among the materials alumina has the least number (and hence density) of observed flaws in the areas shown in Fig. 4a. The same trend was obtained using the Hertzian indentation method (Fig. 2).

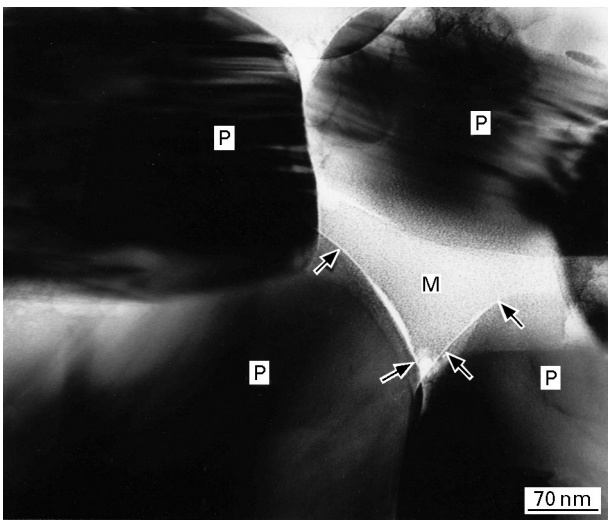

Figure 3 Typical submicrometre-sized cracks observed frequently in the 15 vol % SiC "nanocomposite", but rarely in that with 5 vol % SiC: P, particle; M, matrix.

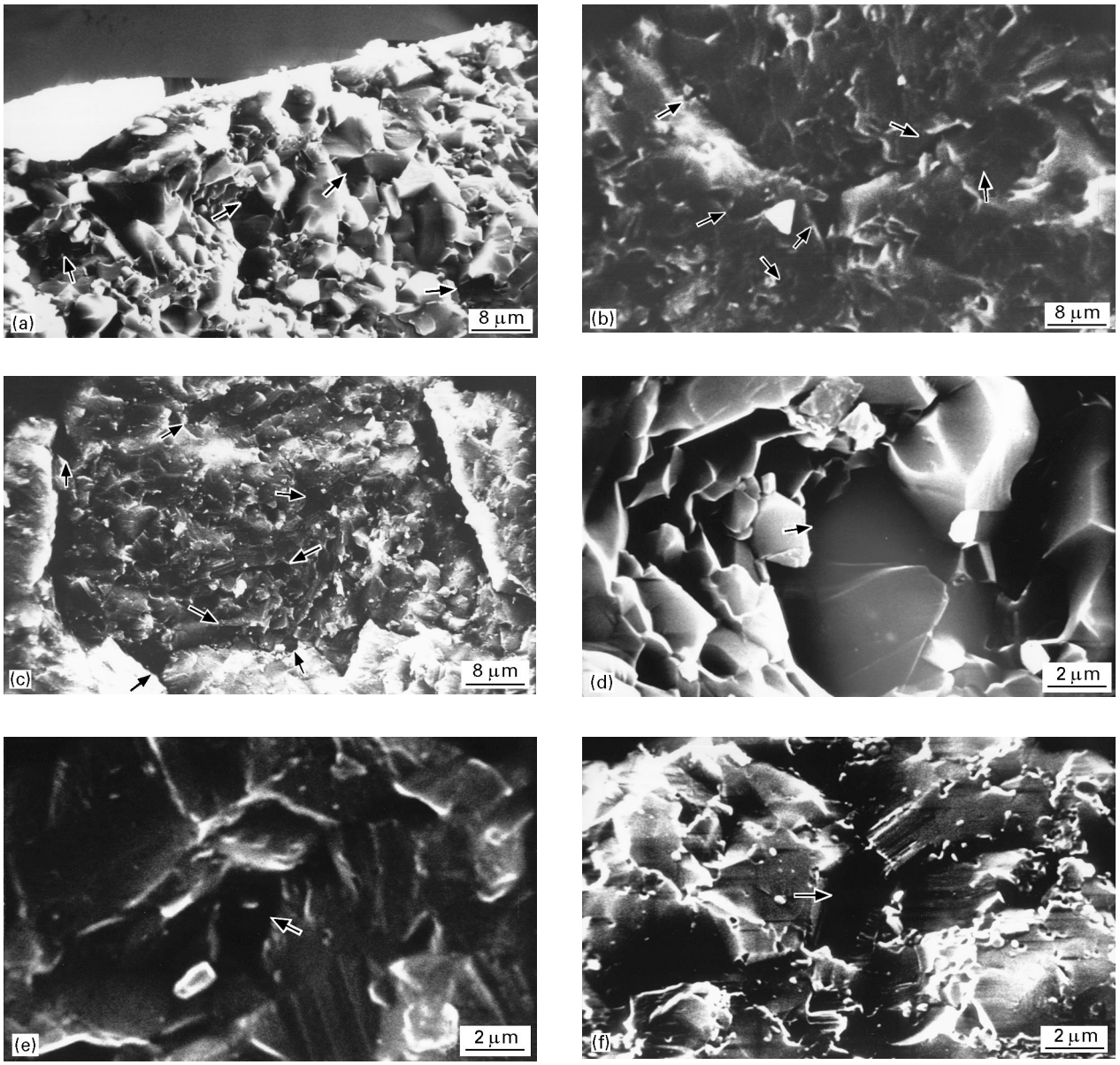

Figure 4 Flaws observed on fracture surfaces for (a) alumina, (b) 5 vol % SiC (c) 15% SiC (all wide area views), and (d) alumina, (e) 5 vol % SiC, (f)15 vol % SiC (all showing typical sizes of largest flaws).

TABLE II Critical (largest) flaw sizes, C of materials obtained by various mehtods

SiC (vol %)	Largest (critical) flaw size, C (μm)			
	Griffith's	Orowan's	Hertzian	Examination of fracture surface
0[a]	21 ± 6	4.3 ± 1	5.16	3.8 ± 0.5
5	20 ± 6	5.1 ± 1.4	4.5	3.5 ± 0.5
15	31 ± 7	6.1 ± 1.1	6.52	5.0 ± 0.4

[a] This sample is composed entirely of Al_2O_3.

Both methods indicate that the size of the largest flaw in the 5 vol % SiC composite is the smallest.

However, the largest sizes predicted by the Hertzian method were not observed on the fracture surfaces. This is probably because their frequencies and densities are very low. Nonetheless, considering that the strength of a material is within a scatter band, a difference of $\leqslant 1.5$ μm between the largest sizes computed from the Hertzian analysis and those observed on the fracture surfaces should fall within this band.

3.4. Prediction of fracture strength

The sizes of the largest (critical) flaws found by using Equation 1, i.e. the Griffith's model, the Hertzian analysis and by examining the fracture surfaces are shown in Table II.

3.4.1. Griffith's model

Flaws of the sizes predicted by this model, as large as they are, should be easily observed under the SEM on the fracture surfaces, but they were not. It could be argued that such large sizes cannot be observed, because, being that large, their densities are very low (as observed with the largest sizes indicated by the Hertzian method), or that, consequent upon catastrophic failure, the largest flaw(s) fell out with chips of the material. However, the very high degree of densification of the materials should make the distribution of the range of flaw sizes in them uniform to a certain extent. Thus, say for the 15 vol % SiC composite, the model predicts ~ 31 μm as the largest size flaw. If this size is not observed for any of the reasons stated above, other sizes close to this should be observed. Incidentally this is not the case; instead there is this huge gap of 26 μm between the observed and the predicted largest flaw size. On the other hand, the largest size found by the Hertzian method conforms to this principle of uniform distribution of ranges of flaw sizes. Hence, though the 6.52 μm size found by the latter method is not observed on the fracture surface, those present are very close to this value.

The critical flaw sizes predicted by using the Griffith's model were obtained using experimental fracture strengths [4] and K_{Ic} values [6] in Equation 1. If, however, the largest flaw sizes predicted by the Hertzian method or observed on the fracture surfaces are introduced into this equation, the resulting fracture strengths of the materials are by far higher than the experimental (four-point bend test) values. Therefore the applicability of Orowan's model was investigated.

3.4.2. Orowan's model

Orowan [12] considered cracks in real materials to be blunt (against Griffith's assumption of sharp cracks). On this consideration, Davidge [7] derived a fracture stress, σ_f, for a material with surface energy for fracture, γ_0, Young's modulus, E, and a critical flaw size, C, as

$$\sigma_f = \left(\frac{E\gamma_0}{8C}\right)^{1/2} \quad (2)$$

However, $(2E\gamma_0)^{1/2}$ gives the fracture toughness, K_{1c}, of a material. Hence Equation 2 can be rewritten as

$$\sigma_f = \frac{K_{Ic}}{4(C)^{1/2}} \quad (3)$$

Introducing the experimental values of σ_f and K_{Ic} from Table I for alumina, 5 and 15 vol % SiC composites in Equation 3, the value of the critical flaw size for each of the materials is calculated. These values are shown in Table II. It can be seen that the sizes predicted by Orowan's model fit well with those observed by the Hertzian method.

Hence a similarity of the distribution of flaws on the fracture surfaces with that found by the Hertzian method is established (Section 3.3). The critical flaw sizes determined by the latter method fit well with those predicted by Orowan's model. Therefore the strengths of these materials (and indeed any real brittle material that generates Hertzian ring cracks) can be predicted by this model, using parameters obtained through relatively fast techniques of Vickers indentation (for fracture toughness) and Hertzian indentation (for critical flaw sizes). The model becomes more compelling if there is enough evidence to prove that the crack-tip is blunt, a problem that a theoretical approach cannot solve exactly [13]. Therefore demonstrable fractographic features are presented below to explain the nature of the crack-tip.

3.5. The nature of the crack-tip

3.5.1. Effect of plastic deformation zone

It is well established [13, 14], and was also observed in this study (Fig. 5), that plastic deformation occurs in zones immediately surrounding indents. The zones extend to about 10 μm from the indent in the composites (Fig. 5b), and to a slightly shorter distance in monolithic alumina (Fig. 5a).

Flaws from which cracks can originate in a fracture process of ceramic materials are many. In analogy to the indents, the immediate zones around crack-originating flaws will also be under plastic deformation. It is possible for a crack that would cause fracture, while propagating, to find its tip in the plastic

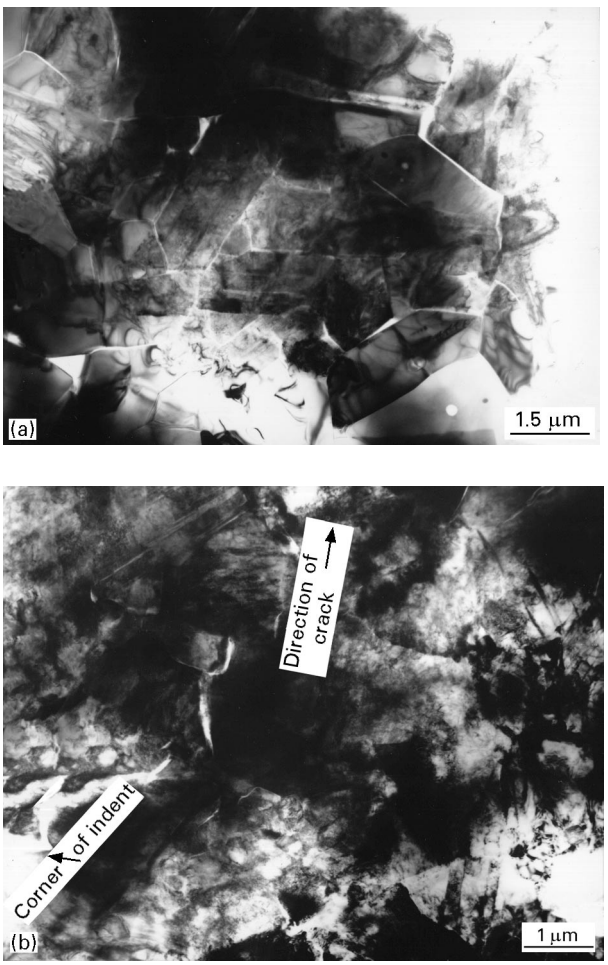

Figure 5 Zones of plastic deformation (dislocations) around Vickers indents made with a 2 N load: (a) alumina and (b) 15 vol % SiC "nanocomposite". Note the distance away from the indent that the zones extend: about 10 μm for the composite, and slightly shorter for alumina.

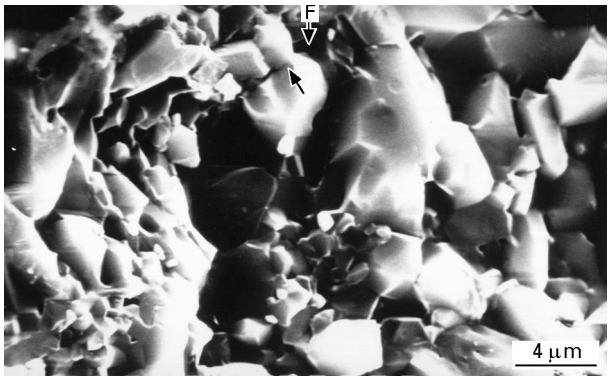

Figure 6 A crack-tip (arrowed) in alumina ~1 μm away from a flaw, F, in its front. In analogy to the case of the indent, this distance is well within a plastic deformation zone.

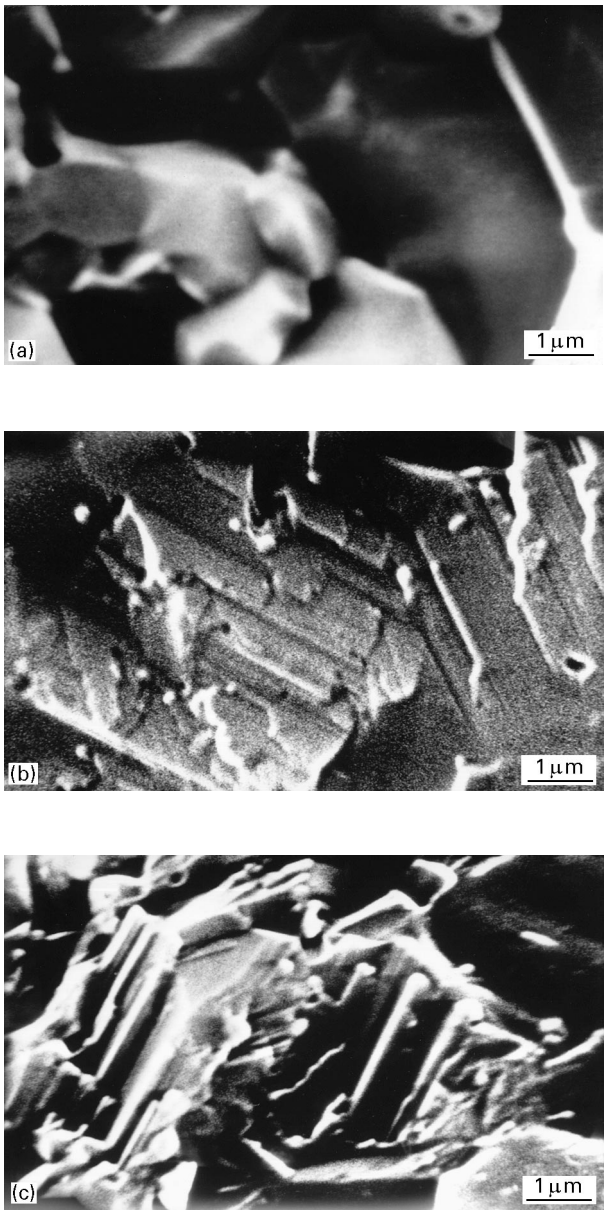

Figure 7 Fracture surfaces of (a) alumina, (b) 5 vol % SiC, and (c) 15 vol % SiC "nanocomposites". Note that the failure is intergranular in alumina, but transgranular in the composites, and also the fact that the interspacing distances of the fracture steps in the 5 vol % SiC composite are farther than those of the 15 vol % SiC composites.

deformation zone of adjacent flaws from which the other cracks originated. An example of this is shown in Fig. 6 for alumina. The crack-tip (arrowed) is found ~ 1 μm away from the flaw, F, in its front, a distance well within the plastic deformation zone immediately around the flaw.

The case just described should not be confused with the activation of pre-existing dislocations, which have been suggested [13] may not blunt the crack-tip. The dislocation atmospheres in Fig. 5a, b are new, and result from the fracture process. They are not those of a pre-existing source. Alumina had virtually no dislocation network prior to the test, while that preexisting in the composites (presented in the next section) was quite different from that shown in Fig. 5b. Therefore the walls of crack-tips found in these zones will not recontact, thereby leading to bluntness of the former.

3.5.2. Effect of fractographic surface details

The presence of fracture steps (usually associated with fringes in TEM) prevent crack walls at the tip from recontacting, thus causing bluntness [13]. Fig. 7 shows SEM micrographs of typical fracture surfaces of alumina (a), 5 vol % SiC (b) and 15 vol % SiC composites (c) [4] used in this study. It can be seen that the composites are full of steps. Fig. 8a is a TEM micrograph of the fringes around the crack-tips (arrowed) in the 15 vol % SiC composite. Hence the crack-tips in the composites can be described as being blunt.

Fringes, and the generation of dislocations characterize the healing of crack interfaces if the crack-tip is sharp [13]. However, in the present study, dislocations are absent around the fringes at the crack-tips of alumina (Fig. 8b). This may suggest that the healing is incomplete, and therefore justifies considering the crack-tip to be blunt. It should be noted that the dislocations in the composite (Fig. 8a) are not as a result of crack-healing, but rather are pre-existing from the sintering stage, as demonstrated in Fig. 8c.

3.6. Limitations of Hertzian flaw analysis

The computer simulation is such that the detectable maximum flaw size is about 16 μm [10]. Because porosity is synonymous to flaws, it is therefore absolutely necessary that the materials to be tested are processed to $\geqslant$ 99% TD. It is also required that the surfaces of the samples to be tested are prepared to a degree that the sizes of the flaws introduced by the surface preparation are smaller than those of the intrinsic ones. This is because the method detects the largest flaw that gives rise to the ring crack. For example, the critical flaw sizes found in the 5 vol % SiC composite are 4.5 μm for 1/4 μm diamond finish (present study), and 6 and 8 μm, respectively, for surface finishes with 3 and 14 μm diamond [6]. The flexural strengths of the 3 and 14 μm diamond finished samples are understandably lower (530 and 458 MPa, respectively) than that of the 1/4 μm diamond finished sample. Ideally, therefore, to ensure that the largest flaws being detected are intrinsic to the material, the

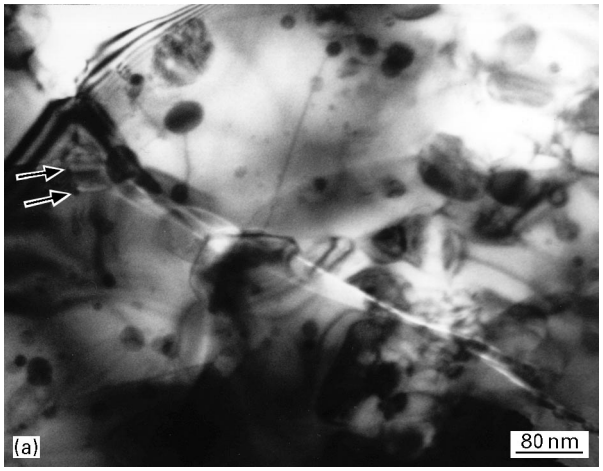

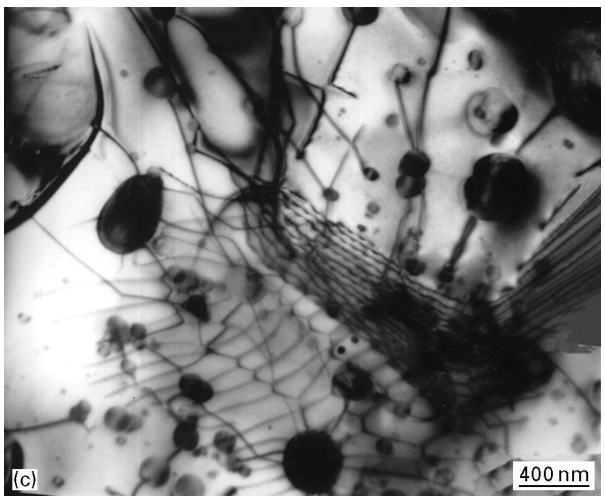

Figure 8 Fringes around (a) the crack-tips (arrowed) of the 15 vol % SiC "nanocomposite", most probably resulting from fracture steps (Fig. 7c), and (b) the crack-tip of alumina (in the absence of dislocations the healing of the crack-tip may be incomplete). (c) Dislocation network obtained in the 15 vol % SiC "nanocomposite" at the sintering stage (this, and not a crack healing process, is the source of the dislocations in Fig. 8a).

surfaces should be finish-polished down to $\leqslant 1\,\mu m$ diamond.

The statistics of the flaws are very much dependent on the fracture loads, which in turn are affected by the elastic constants of the both the indenter and the substrate materials. As much as possible, the latter should be similar. This is because the effect of a very high mismatch in elastic constants (for example, steel or tungsten carbide on glass) on fracture loads is not negligible [15]. Generally, more compliant indenter materials (relative to those of the substrate) lead to lower fracture loads, and vice versa, than would be if both materials are elastically similar [16].

The "searched area" in the computer simulations of the analysis is appreciably an overestimate of real flaw distributions, because it is considered that all the flaws are normal to the radial direction of the indenter [10]. However, there is no particular mode of flaw distribution in the real materials. Therefore, although the results in the present study are compelling, further confirmation of the validity of flaws determined (on well processed ceramic bodies) by the Hertzian indentation method representing (their) intrinsic flaws is still needed.

3.7. Prediction of the comparative strength of the materials

A calculated decrease of critical flaw size from 23 (for alumina) to 6 μm (for Al_2O_3–SiC "nanocomposites") was suggested [1] to be responsible for the higher strength of the latter. On the basis of Equation 1 or 3, the increase in strength of the composite was also partly attributed [1] to an increase in toughness, K_{Ic}.

However, the observed flaws on the fracture surfaces of both alumina and the composites in the present work are approximately of the same size (Fig. 4), with the only difference being the density of flaws. The Hertzian analysis shows that the critical flaw size of the 15 vol % SiC composite is the largest (6.52 μm), while for all practical purposes the 4.5 μm flaw of the 5 vol % SiC composite should be regarded as equivalent to the 5.16 μm flaw of alumina. If flaw size is the controlling factor, the strength of the 15 vol % SiC composite should have been lower than that of alumina, but it is not (see Table I). The strengthening may also be independent of the toughening achieved by the change in fracture mode from integranular (alumina) to transgranular (composites). This is because, as Table I shows, although the 15 vol % SiC composite is tougher than the 5 vol % SiC composite (a phenomenon also demonstrated using crack paths studied under the TEM [4]), the strength of the latter is higher. The same fracture toughness value has also been demonstrated [17] to give different flexural strengths in alumina samples (same composition) densified to the same degree, but only varying in grain size.

Therefore flaw size may not be a good indicator with which to compare the strengths of materials showing different fracture modes. Even when the fracture mode is the same (as in the composites of the present work, or alumina of [15]), flaw size differences could partly explain the variation in strength, but a full account can only be obtained if other fractographic features are simultaneously considered. For instance, if the fracture strengths of the 5 and 15 vol % SiC composites are calculated using the critical flaw sizes from the Hertzian analysis and Equation 3, it will

be seen that the flaw size factor accounts for about 14% of the actual experimental difference of 18%.

This extra strengthening may be attributable to the longer separation distances of the fracture steps of the 5 vol % SiC composite, relative to those of the 15 vol % SiC composite (Fig. 7b and c, respectively). This is because longer separation distances imply [18] taller step heights, and the latter have been shown [19] to lead to higher fracture strengths. The cause and presence of these steps are therefore responsible for the higher strength of all the composites relative to alumina, while the smaller separation distances of the steps in the 15 vol % composite are partly responsible for the reduction in strength of the latter, in comparison with that of the 5 vol % composite.

4. Conclusions

The modal sizes of the flaws found on the fracture surfaces of four-point bent samples match very well with those determined by the Hertzian indentation analysis. The experimental fracture strengths of the materials are reasonably well predicted using the critical flaw sizes found by the latter method and Orowan's model.

The effect of deformation zones around indents (flaws), from which cracks originate, and fractographic surface details support the concept of blunt crack-tips, thus rationalizating the preference of Orowan's model to that of Griffith.

Further confirmation of the applicability of the Hertzian indentation analysis for determining the sizes and densities of intrinsic flaws in brittle materials is necessary. This requires materials processed to $\geqslant 99\%$ TD, and that the surface preparation medium does not introduce flaws of sizes larger than the intrinsic ones.

Both micrographic and analytical methods reveal that the flaw sizes of alumina and the 5 vol % SiC composite are practically the same. Therefore the change in mode of fracture from intergranular (alumina) to transgranular (composites), and not flaw size, is more appropriate for explaining the strengthening observed in the latter. The flexural strength of the 15 vol % SiC composite is lower than that of 5 vol % SiC, because of the shorter separation distances (implicitly shorter heights) of the fracture steps of the former.

Acknowledgements

This project was sponsored by the EPSRC, UK. Comments by Dr. S. G. Roberts of Department of Materials, University of Oxford are acknowledged.

References

1. K. NIIHARA, *J. Ceram. Soc. Jpn* **99** (1991) 974.
2. J. ZHAO, L. C. STEARNS, M. P. HARMER, H. M. CHAN and G. A. MILLER, *J. Amer. Ceram. Soc.* **76** (1993) 503.
3. C. E. BORSA, S JIAO, R. I. TODD and R. J. BROOKS, *J. Microsc.* **177** (1995) 305.
4. C. C. ANYA and S. G. ROBERTS, *Acta Mater.* to be published.
5. C. C. ANYA and S. G. ROBERTS, *J. Euro. Ceram. Soc.* **17** (1997) 565.
6. *Idem., ibid.* **16** (1996) 1107.
7. R. W. DAVIDGE, "Mechanical behaviour of ceramics" (Cambridge University Press, Cambridge, 1986) p. 31.
8. M. SAKAI and R. C. BRADT, *Int. Mater. Rev.* **38** (1993) 53.
9. J. D. POLONIECKI and T. R. WILSHAW, *Nature* **229** (1971) 226.
10. P. D. WARREN, D. A. HILLS and S. G. ROBERTS, *J. Hard Mater.* **5** (1994) 213.
11. I. LEVIN, W. D. KAPLAN, D. G. BRANDON and T. WEIDER, *Acta Metall. Mater.* **42** (1994) 1147.
12. E. OROWAN, "Fatigue and fracture of metals" (MIT Press, Cambridge, MA, 1950) p. 139.
13. B. R. LAWN, B. J. HOCKEY and S. M. WIEDERHORN, *J. Mater. Sci.* **15** (1980) 1207.
14. B. J. HOCKEY, *J. Amer. Ceram Soc.* **54** (1971) 223.
15. P. D. WARREN, *J. Euro. Ceram. Soc.* **15** (1995) 201.
16. K. L. JOHNSON, J. J. O'CONNOR and A. C. WOODWARD, *Proc. R. Soc. Lond.* **A334** (1973) 95.
17. M. YASUOKA, K. HIRAO, M. E. BRITO and S. KANZAKI, *J. Amer. Ceram. Soc.* **78** (1995) 1853.
18. F. F. LANGE and K. A. D. LAMBE, *Phil. Mag.* **18** (1968) 129.
19. J. J. GILMAN, *J. Appl. Phys.* **27** (1956) 1262.

Received 4 December 1996
and accepted 1 September 1997